Molecular Pharmacology Fast Forward. Published on April 4, 2011 as doi: 10.1124/mol.111.071688
This article has not been copyedited and formatted. The final version may differ from this version.

Mechanisms of Modal Activation of GluA3 Receptors

Kinning Poon, Ahmed H. Ahmed, Linda M. Nowak,[1] and Robert E. Oswald[1]

Department of Molecular Medicine, Cornell University, Ithaca, NY 14853

Molecular Pharmacology Fast Forward. Published on April 4, 2011 as DOI: 10.1124/mol.111.071688
This article has not been copyedited and formatted. The final version may differ from this version.

a) Running title: Modal activation of GluA3 Receptors

b) Correspondence to:

Robert E. Oswald
Department of Molecular Medicine
Cornell University
Ithaca, NY 14853
607-253-3877
607-253-3659 (FAX)
reo1@cornell.edu

c) Manuscript size:

Number of text pages:	35
Number of tables:	4
Number of figures:	7
Number of words in the Abstract:	248
Number of words in the Introduction:	689
Number of words in the Discussion:	1495

d) Abbreviations

AMPA, α-amino-3-hydroxy-5-methyl-4-isoxazole-propionic acid; CTZ, cyclothiazide (6-Chloro-3,4-dihydro-3-(5-norbornen-2-yl)-2*H*-1,2,4-benzothiazidiazine-7-sulfonamide-1,1-dioxide); flipped/unflipped peptide bond, a 180˚ flip of the D655/S656 peptide bond (GluA3) upon binding of agonist can result in the formation of H-bonds between S656 (Lobe 2) and G453 (Lobe 1), and between D655 and Y452 through a water molecule; FW, (*S*)-5-fluorowillardiine ((S)-(-)-α-Amino-5-fluoro-3,4-dihydro-2,4-dioxo-1(2H)pyridinepropanoic acid); NO_2W, (*S*)-5-nitrowillardiine ((S)-(-)-α-Amino-5-nitro-3,4-dihydro-2,4-dioxo-1(2H)pyridinepropanoic acid); ClW, (*S*)-5-chlorowillardiine ((S)-(-)-α-Amino-5-chloro-3,4-dihydro-2,4-dioxo-1(2H)pyridine-propanoic acid); GluA1-4, four subtypes of AMPA receptor; $GluA2_o$, flop form of GluA2; $GluA3_i$, flip form of GluA3; LBD, extracellular ligand-binding domain of GluA2 and GluA3; LL, log likelihood; MIL, maximum likelihood interval; NMDA, N-methyl-D-aspartic acid; RDC,

Molecular Pharmacology Fast Forward. Published on April 4, 2011 as DOI: 10.1124/mol.111.071688
This article has not been copyedited and formatted. The final version may differ from this version.

residual dipolar coupling; SKM, segmental-k-means; UBP282, ((αS)-α-Amino-3-[(4-carboxyphenyl)methyl]-3,4-dihydro-2,4-dioxo-1(2H)-pyrimidinepropanoic acid).

Molecular Pharmacology Fast Forward. Published on April 4, 2011 as DOI: 10.1124/mol.111.071688
This article has not been copyedited and formatted. The final version may differ from this version.

Abstract

AMPA receptors are the major excitatory neurotransmitter receptors in the CNS and are involved in numerous neurological disorders. An agonist-binding site is present in each of four subunits that form a functional channel. Binding consists of three steps: docking of agonist to the bi-lobed ligand binding domain (LBD), closure of the LBD, and increased stability of the closed-lobe conformation through interlobe hydrogen bonding. We describe GluA3 single channel currents activated by nitrowillardiine (NO_2W) and chlorowillardiine (ClW) in the presence of cyclothiazide, in conjunction with crystal structures of GluA2 and GluA3 LBDs bound to fluorowillardiine (FW), ClW, and NO_2W. When bound to NO_2W or ClW, the GluA3 channel opens to three conductance levels with comparable open probabilities and displays modal behavior similar to that obtained with glutamate and FW as agonists (Poon et al., 2010). At lower concentrations, ClW evoked an alternate kinetic behavior, consisting of high open probability in lower conductance states. The structure of ClW bound to GluA3 LBD exhibits a unique partially open hydrogen bonding structure that may be associated with these alternative kinetics. NO_2W evoked longer open times than seen for other agonists in high and very high modes. The structure of GluA2 LBD bound to NO_2W exhibits fully closed lobes with additional interlobe interactions mediated by the nitro group. Beyond differences in efficacy between full and partial agonists, the complexities of the single channel behavior of AMPA receptors may also be associated with small interactions that modify the stability of various degrees of closure.

Molecular Pharmacology Fast Forward. Published on April 4, 2011 as DOI: 10.1124/mol.111.071688
This article has not been copyedited and formatted. The final version may differ from this version.

Introduction

AMPA receptors, a class of ionotropic glutamate receptors expressed in CNS neurons and glial cells, are involved in rapid excitatory synaptic transmission and plasticity (Citri and Malenka, 2008; Derkach et al., 2007) and in neurological diseases (Heath and Shaw, 2002; Hynd et al., 2004; Liu and Zukin, 2007). They are formed as tetrameric combinations of GluA1-4 subunits (Dingledine et al., 1999). A single subunit consists of an extracellular N-terminal domain, a ligand-binding domain (LBD), pore-forming transmembrane domains, and a cytoplasmic C-terminal domain. AMPA receptors can also bind allosteric modulators, such as cyclothiazide, which block desensitization. In contrast to NMDA receptors, whose activation is highly cooperative (Banke and Traynelis, 2003; Kussius and Popescu, 2009), AMPA receptor conductance increases in discrete steps as agonist concentration is increased (Rosenmund et al., 1998; Smith and Howe, 2000), consistent with each subunit binding an agonist molecule and contributing to channel activation (Dingledine et al., 1999; Traynelis et al., 2010). Recently, detailed single channel studies have begun to address the molecular mechanisms of AMPA receptor-channel activation (Jin et al., 2003; Poon et al., 2010; Prieto and Wollmuth, 2010; Smith and Howe, 2000).

Characterization of AMPA receptor structure and function has led to initial models of channel activation. Specifically, the closure of the LBD upon agonist binding has been directly correlated to activation of the gating mechanism (Armstrong and Gouaux, 2000). Early studies correlated the degree of LBD closure in crystal structures to the amplitude of whole cell currents at saturating agonist concentrations. Full agonists exhibited the most closure and, in comparison, partial agonists exhibited partial closures (Jin et al., 2003). However, NMR studies and crystal structures of mutant GluA2 LBDs have suggested that the stability of the closed lobe may also contribute to agonist efficacy. Agonist binding consists of at least three steps: (1) binding to Lobe 1, (2) closure of the lobes and contacts with Lobe 2, and (3) interlobe contacts (including H-bonds) to stabilize the closed lobe form (Abele et al., 2000; Armstrong and Gouaux, 2000;

Molecular Pharmacology Fast Forward. Published on April 4, 2011 as DOI: 10.1124/mol.111.071688
This article has not been copyedited and formatted. The final version may differ from this version.

Fenwick and Oswald, 2010; Robert et al., 2005; Weston et al., 2006; Zhang et al., 2008a; Cheng et al., 2005). Lobe closure is required for channel gating, but the degree of lobe closure that can trigger gating is not clear (*i.e.*, does gating require a full closure?) and the role of auxiliary interlobe contacts has not been completely resolved. In addition, Prieto and Wollmuth (2010) suggest that cooperativity arising from intersubunit contacts may play a role in gating and modal behavior.

Long single channel recordings can capture details of subtle channel behaviors, which were analyzed using state models that describe measurable protein transitions during activation steps and which were, in turn, correlated to changes in the LBD. Our previous studies found that glutamate (full agonist) and FW (strong partial agonist) activated the GluA3 channel to three similar conductance levels with glutamate-activated channels favoring higher conductance states, and at least five modes of channel activity, defined by open probability, were observed (Poon et al., 2010). These modes were seen for both glutamate and FW, with the full agonist, glutamate, favoring those modes that had higher open probability. Given the complexity observed with a full agonist and a strong partial agonist, two slightly weaker partial agonists were tested to determine if the modal behavior was similar to the stronger partial agonist and if further complexities in channel gating could be observed. The studies described here show a larger spectrum of activity using two additional partial agonists in the willardiine family, nitrowillardiine (NO_2W) and chlorowillardiine (ClW). Although the crystal structures we obtained of FW and ClW bound to the LBD of GluA3 and for NO_2W and ClW bound to GluA2 are similar to most published AMPA LBD structures, several details differ that may be related to the responses elicited by NO_2W and ClW. Details that vary upon binding of different ligands are the orientation of the two lobes, the orientation of the peptide bond between D655 and S656, and the orientation of the sidechain of M712.These interactions within the LBD may contribute to differences in single channel activity of GluA3 receptors when bound to either strong or weak partial agonists.

Molecular Pharmacology Fast Forward. Published on April 4, 2011 as DOI: 10.1124/mol.111.071688
This article has not been copyedited and formatted. The final version may differ from this version.

Methods

Cell culture

Human embryonic kidney (HEK) 293 cells were stably transfected with GluA3i-G (S.M. Holley & L.M. Nowak, unpublished), and clonal stable cell lines were established. The receptor is the flip variant, and has a G in the R/G editing site. The cells were cultured in Dulbecco's Modified Eagle's Medium (DMEM) containing 10% fetal bovine serum (FBS), 1% penicillin-streptomycin and 1 µg/mL blasticidin, pH 7.4. The addition of the antibiotic, blasticidin, in the culture media selects for the growth of cells that express GluA3 channels. Cells were passaged every 3-4 days and used within 48 hours after passage. All cultures were maintained in a 37°C incubator with 5% CO_2.

Acquisition of Single Channel Currents

All experiments were performed at room temperature (~23°C). Pipettes were pulled from thick-walled borosilicate glass with filament (Sutter Instrument Company, Novato, CA, USA) and firepolished to a resistance of 15-20 MΩ. Solutions were buffered at pH 7.4 and filtered using a 2 µm sterile filtering system (Corning, Lowell, MA). The bath buffer was a Ca^{2+}/Mg^{2+}-free Dulbecco's phosphate saline buffer with 1.0 mM added $MgCl_2$ (Invitrogen, Carlsbad, CA). The pipette solution contained (in mM): 150 NaCl, 2 KCl, 10 Hepes/NaOH (pH 7.4). Stock solutions of NO_2W or ClW (Tocris Bioscience, Ellisville, MO, or Ascent Scientific, Princeton, NJ), dissolved in the pipette solution, were kept frozen in aliquots at -20°C until the day of the experiment. Cyclothiazide (CTZ; Tocris Bioscience, Ellisville, MO, or Ascent Scientific, Princeton, NJ) was dissolved in methanol (50 mM stock solution) and stored at -20˚C. CTZ was added (100-150 µM) to all agonist containing pipette solutions, and the solutions were used for less than two hours.

Single channel currents were amplified at a gain of 100 mV/pA with an EPC-7 amplifier, low-pass filtered to 10 kHz using an external 8-pole Bessel filter, and digitized at 20 kHz using

Molecular Pharmacology Fast Forward. Published on April 4, 2011 as DOI: 10.1124/mol.111.071688
This article has not been copyedited and formatted. The final version may differ from this version.

pClamp 7 software (Molecular Devices, Sunnyvale, CA). Single channel currents were recorded for 2 to 10 minutes in the cell-attached mode with pipette holding potentials of +80 to +120 mV. Data were converted from abf to qdf format on QuB software (www.qub.buffalo.edu) for analysis.

Analysis of Single Channel Data

Only data from patches with one channel were used for analysis. A segment of the record without channel activity was used to define the baseline in QuB. As described previously (Poon et al., 2010), we tested the number of open conductance levels by idealizing the data assuming up to four different conductance levels, filtering at frequencies ranging from 1 to 10 kHz, and altering the dead time using a range from 50-200 μs. The results from different combinations of criteria were then analyzed, and the criteria that provided the best fits to the amplitude histogram, dwell time histograms, and the largest log likelihood (LL) units were used for all subsequent analyses. Three open conductance levels provided the best fits to the data, and the addition of a fourth open conductance level consistently exhibited a lower LL, despite the increase in free parameters (Poon et al., 2010). All data were initially idealized at a dead time of 150 μs using the segmental-k-means (SKM) algorithm (Qin et al., 1996) to an initial simple linear model consisting of one closed and three open classes (C↔O1↔O2↔O3) starting with all rates set to 100 s^{-1}. The data were analyzed with or without an additional 5 kHz filtering (effective filter of 4.5 kHz). A dead time of 200 μs was imposed on patches that had additional filtering. Maximum interval likelihood (MIL) analysis (Qin et al., 1996) was applied on this initial model to determine the fit to the dwell time histograms. States were then added one at a time to each closed and open class, re-idealized, refitted using MIL, and retained if the fits to the histograms improved and/or if the LL units increased by >10. If the addition of a state increased the LL by 10, but the rates to the new state were either close to zero or unrealistically fast, the additional state was omitted. This process was repeated again with rates starting at 10 s^{-1} to confirm that the final model and the final rates were not affected by the starting values. Similar to Poon et al.

Molecular Pharmacology Fast Forward. Published on April 4, 2011 as DOI: 10.1124/mol.111.071688
This article has not been copyedited and formatted. The final version may differ from this version.

(2010), our final model consists of three closed states and two open states in each of the open conductance levels (Figures 1A & 3). Loops that connected closed states to the intermediate or large conductance levels in the model were tested, but in most cases worsened the fit to the dwell time histograms and/or gave unrealistic rates, so loops were not considered in our final model. Based on the transition matrices (Figure 1B), transitions between the closed and the intermediate or large conductance levels were infrequently observed. Therefore, the final model does not include these transitions.

Modal behavior was determined by segmenting the data based on the closed probability as described in Poon et al. (2010). Patches with long closures were modeled using four or five closed states. The critical time (t_{crit}), which describes the minimum closed duration between two bursts (Magleby and Pallotta, 1983), was used to discard long closures. The resulting clusters of openings and closings were re-idealized to an SKM model with one closed and three open conductance classes to determine the closed and open probabilities of each segment. The select function in QuB was then used to sort the segments into modes. The X-means algorithm (Pelleg and Moore, 2000) places each segment into the appropriate mode using the closed time probability (P_c; P_c was used in this step because of the multiple conductance levels). The number of modes was determined by sorting the segments into similar clusters based on the value of X until the assignments stabilized. The sorted modes were analyzed individually using the model described above. In a few records having only three closed states and one mode, the model in Figure 1A was applied to the entire record. The dwell times of similar modes were averaged, but each mode was modeled separately. Because the number of events in each group was necessarily less than the total number of events in the record, the LL was normalized to the number of events (LL/event) and each group was compared to the whole record. Based on the analysis using the X-means algorithm described above, five distinct modes (VL, very low; L, low; M, medium; H, high; VH, very high) were observed as detailed in Poon et al. (2010) for glutamate and FW.

Molecular Pharmacology Fast Forward. Published on April 4, 2011 as DOI: 10.1124/mol.111.071688
This article has not been copyedited and formatted. The final version may differ from this version.

Once the record was divided into modes, an "efficacy factor" (Jin et al., 2003; Poon et al., 2010; Prieto and Wollmuth, 2010) was determined based on a binomial distribution. Once bound with 2 to 4 agonist molecules, the channel can display openings to up to three conductance levels. The four levels (closed plus three open) can be viewed as four trials (n) and the level of a particular opening is defined as the number of successes (k). The probability of success ("efficacy factor") can then vary between agonist, at different concentrations, and, in this case, in different modes.

Protein Preparation and Purification

GluA2 LBD consists of residues N392 - K506 and P632 - S775 of the full rat $GluA2_o$ subunit (Hollmann and Heinemann, 1994), a 'GA' segment at the N-terminus, and a 'GT' linker connecting K506 and P632 (Armstrong and Gouaux, 2000). A similar construct of $GluA3_i$ LBD was prepared as described previously (Ahmed et al., 2009b). pET-22b(+) plasmids were transformed in *E. coli* strain Origami B (DE3) cells and were grown at 37˚C to OD600 of 0.9 to 1.0 in LB medium supplemented with the antibiotics (ampicillin and kanamycin). The cultures were cooled to 20˚C for 20 min and isopropyl-β-D-thiogalactoside (IPTG) was added to a final concentration of 0.5 mM. Cultures were allowed to grow at 20˚C for 20 h. The cells were then pelleted and the LBD purified using a Ni-NTA column, followed by a sizing column (Superose 12, XK 26/100). The final purification step used an HT-SP-ion exchange-Sepharose column (Amersham Pharmacia). Glutamate (1 mM) was maintained in all buffers throughout purification. After the last column, the protein was concentrated and stored at 4˚C in 20 mM sodium acetate, 1 mM sodium azide, and 10 mM glutamate at pH 5.5.

Crystallography

For crystallization trials, the ligand was exchanged by successive dilution and concentration, and the protein was subsequently concentrated to 0.2-0.5 mM using a Centricon 10 centrifugal filter (Millipore, Bedford, MA). Crystals were grown at 4˚C using the hanging

Molecular Pharmacology Fast Forward. Published on April 4, 2011 as DOI: 10.1124/mol.111.071688
This article has not been copyedited and formatted. The final version may differ from this version.

drop technique, and the drops contained a 1:1 (*v*/*v*) ratio of protein solution to reservoir solution. The reservoir solution contained 14-15% PEG 8K, 0.1 M sodium cacodylate (pH 6.5), 0.1-0.15 M zinc acetate, and 0.25 M ammonium sulfate. The final concentrations of agonists were: FW, 2 mM; NO_2W, 2 mM; and ClW, 2 mM.

Data were collected at the Cornell High Energy Synchrotron Source beam line A1 using a Quantum-210 Area Detector Systems charge-coupled device detector. Data sets were indexed and scaled with HKL-2000 (Otwinowski and Minor, 1997). Structures were solved with molecular replacement using Phenix (Adams et al., 2002). Refinement was performed with Phenix (Adams et al., 2002), ccp4 (Collaborative_Computational_Project, 1994), and Coot 0.6.1 (Emsley and Cowtan, 2004) was used for model building.

Results

Single Channel Behavior of GluA3 Activated by NO_2W and ClW

NO_2W and ClW activate GluA3 channels in the same manner as glutamate and FW: Members of the willardiine family of partial agonists share the same overall structure but differ in the substituent in the 5-position. They produce a graded level of whole-cell activation dependent on the size and electronegativity of the substituent, with electronegativity seemingly affecting ligand potency and the size apparently affecting efficacy (Patneau et al., 1992). Efficacy followed the pattern: FW > NO_2W > ClW (Patneau et al., 1992). Despite differences in efficacy, our single channel studies, using agonist concentrations which range from >EC_{50} to saturating levels, show the willardiine compounds all activate the homomeric GluA3 receptor to three conductance levels. NO_2W and ClW activated GluA3 channels to three open levels with conductances of: 16 ± 0.7, 29 ± 1.6, 40 ± 1.4 pS for NO_2W (n=4); and 15 ± 0.9, 25 ± 1.4, 38 ± 1.4 pS for ClW (n=4) similar to those reported by Poon et al. (2010) for glutamate and FW. A representative trace showing single channel currents in 100 µM NO_2W is presented in Figure 2A. Amplitude histograms for 500 µM NO_2W and 500 µM ClW are shown in Figures 2B and C,

Molecular Pharmacology Fast Forward. Published on April 4, 2011 as DOI: 10.1124/mol.111.071688
This article has not been copyedited and formatted. The final version may differ from this version.

respectively, for receptors activating in a Very High (VH) mode (see Methods for a detailed explanation of the modal behavior). As shown in Table 1, the population of each conductance level is similar for NO_2W and ClW in VH mode.

The simple model derived from studies with glutamate and FW fit the data well (Figure 1A). Figure 3 shows dwell time histograms for the 500 μM NO_2W and ClW data. The closed histogram was fit by the sum of three exponentials and the open histograms for each conductance level were fit by two exponentials, as reported for glutamate and FW activation of the GluA3 receptor (Poon et al., 2010). Based on state transition matrices (Figure 1B), the channel preferentially transitions between adjacent conductance levels, when bound to NO_2W and ClW. These results suggest the mechanism of activation with NO_2W and ClW, like FW, is similar to glutamate.

Although the frequency of the channel to enter a specific mode is dependent on the agonist concentration, the activity within a mode was the same and independent of agonist concentration. For this reason, and as done previously (Poon et al., 2010), the probability of populating each conductance level was averaged for the VH mode for each agonist at a saturating concentration to obtain a more global picture of the occupation of specific conductance levels for NO_2W and ClW compared to FW and glutamate (Table 1). All three willardiines have very similar open probabilities in all conductance levels. ClW and NO_2W populate the highest conductance level to a lesser extent than glutamate ($p < 0.05$). NO_2W and ClW spend a similar percentage of time in the largest conductance level ($p > 0.05$). The population in the intermediate conductance level is lower for NO_2W than for FW ($p < 0.05$). The rank order of the population of the largest conductance level is: ClW $\leq$ NO_2W $\leq$ FW < glutamate. The slightly higher efficacy of FW compared to NO_2W seems to be caused by a higher open probability in O_2. These findings correlate well with the efficacy measured in whole cell recordings (Patneau et al., 1992) and also suggests that efficacy differences of partial

Molecular Pharmacology Fast Forward. Published on April 4, 2011 as DOI: 10.1124/mol.111.071688
This article has not been copyedited and formatted. The final version may differ from this version.

agonists in whole cell studies can be attributed to the differences in open probability in each of the conductance levels (Jin et al., 2003; Poon et al., 2010).

NO_2W and ClW induce modal behaviors: Modal gating of AMPA receptors has been previously described in detail for GluA3 bound to FW or glutamate and was correlated to the hydrogen bonding of the flipped peptide conformation of D655 and S656 to Y452 and G453 (Poon et al., 2010). Modal gating has also been reported for other AMPA (Prieto and Wollmuth, 2010) and for NMDA receptor subtypes (Popescu and Auerbach, 2003; Zhang et al., 2008b). Silberberg et al. (1996) also observed time-dependent changes in P_o for the Ca^{2+}-activated K^+ channels from *Drosophila* (dSlo) and referred to this behavior as "Wanderlust Kinetics." We tested whether modal gating could also be observed for the lower efficacy partial agonists NO_2W and ClW. Patches with long closures were segmented according to the t_{crit} (values ranging from: 1 mM, 79 ms; 500 µM, 82 -226 ms; 100 µM, 49-170 ms; 50 µM, 50-280 ms for ClW; 1 mM, 78 ms, 500 µM, 127-295 ms; 100 µM, 81-180 ms; 50 µM, 131-169 ms for NO_2W) and sorted into the closest P_c distribution using the X means method (Pelleg and Moore, 2000; Poon et al., 2010). These sorted segments were then reanalyzed using the model in Figure 1A. NO_2W and ClW each exhibited five modes of behavior. Modes were obtained by determining whether the channel was open to any level using $1 - P_c$ as in Poon et al., (2010) and they are represented here by P_o (where $P_o = 1 - P_c$) of: 80-100%, 60-79%, 40-59%, 20-39%, and <20% corresponding to Very High (VH), High (H), Medium (M), Low (L) and Very Low (VL) modes, respectively (Figure 4). Patches were also recorded in which a specific mode of activity was retained throughout the record, independent of agonist concentration. The kinetic data acquired from these patches were averaged with other similar P_o modes of behavior.

The single channel behavior of ClW and NO_2W follows a binomial distribution, similar to FW and glutamate, where the probability of success is referred to as an "efficacy factor" (Jin et al., 2003). Figure 5 shows the efficacy factors in each mode (averaged over concentration) for the willardiine derivatives and glutamate. The efficacy factors remain constant for a given mode

Molecular Pharmacology Fast Forward. Published on April 4, 2011 as DOI: 10.1124/mol.111.071688
This article has not been copyedited and formatted. The final version may differ from this version.

regardless of concentration, and are similar for ClW and NO_2W in the V and VH modes. It appears that the efficacy factors for NO_2W are lower than other agonists in the M, L, and VL modes, but this may be due to the small sample size in these modes for NO_2W; in comparison to ClW, most of the M, L and VL activity for NO_2W are of short duration. As expected, glutamate efficacy is higher than that for the willardiine derivatives.

The equilibrium constants associated with the model (Figure 1A) also show differences among modes. The K_{eq} for both ClW and NO_2W favor channel opening to the smallest conductance level in all modes with the exception of L and VL modes, and K_{C1O} decreases from VH to VL modes (Table 2). K_{eq} is a forward equilibrium constant so that a value greater than 1 indicates a relatively greater population of, for example, O_2 than O_1. In the VH mode, the K_{O12a} for NO_2W and ClW is greater than 1 for the transition between the smallest to the intermediate conductance levels. This is in contrast to transitions to the highest conductance level, which are less than 1 (K_{O23a}). For both agonists, K_{eq} to each open state (K_{C1O}, K_{O12a}, and K_{O23a}) decreases as the modal behavior descends in activity (*i.e.*, P_o decreases).

ClW causes alternate kinetic behaviors at lower concentrations of agonist: Channel activity with ClW generally follows the same modal pattern as with glutamate; however, an anomaly was detected in the H mode. ClW seems to exhibit two populations of activity, one with a higher percentage of time in the largest conductance level (P_{O3} of 10-13%; n = 6) and another with a very low P_{O3} (0.17 to 2%; n = 5). In Figure 5A, two efficacy factors are shown for ClW in H mode, with the closed circle and dotted line reflecting the alternate kinetic behavior. Figure 5B displays an example of ClW activation of channels in H mode with a low P_{O3}. In the presence of both ClW and NO_2W, channels were also observed that open largely to the smallest conductance level, with occasional transitions to the middle conductance (Supplemental Table 1). FW was shown previously to produce similar behavior (Poon et al., 2010). The alternative kinetics produced by ClW that give rise to the lower efficacy observed in H mode in Figure 5 may or may not be a result of the same processes that produce sustained openings to only the lowest

Molecular Pharmacology Fast Forward. Published on April 4, 2011 as DOI: 10.1124/mol.111.071688
This article has not been copyedited and formatted. The final version may differ from this version.

conductance level. In any event, it seems clear that partial agonists can be locked into lower conductance states over relatively long periods (up to minutes).

NO_2W produces long dwell times: Similar to previous results with glutamate and FW, the dwell times in the open states of all conductance levels measured with NO_2W and ClW are longer in the VH modes and shorten with a decrease in modal activity (Table 3). The longest dwell time (the second time constant, τ_{O1b}, τ_{O2b}, and τ_{O3b}) in each of the conductance levels in the VH mode for NO_2W is longer than that observed for ClW ($p < 0.05$). τ_{O1b}, τ_{O2b}, and τ_{O3b} for NO_2W ranged from 4-45 ms for all three conductance levels. τ_{O1b}, τ_{O2b}, and τ_{O3b} for ClW ranged from 2-12ms. Comparing this with previous findings (Poon et al., 2010); τ_{O1b}, τ_{O2b}, and τ_{O3b} for glutamate were similar to ClW, ranging from 2-6 ms, whereas FW ranged from 5-28 ms. The order of τ_{O1b}, τ_{O2b}, and τ_{O3b} in decreasing length is: NO_2W > FW > ClW > glutamate.

Summary. The single channel analysis of GluA3 activated by NO2W and ClW displays modal behavior as seen previously for FW and glutamate (Poon et al., 2010). In addition, ClW displays a lower efficacy at times in the H mode, and NO_2W exhibits relatively long dwell times in the VH mode.

Structures of GluA2 and GluA3 bound to FW, NO_2W and ClW

Lobe closure variability: When bound to various agonists, the GluA3 and GluA2 LBD structures are quite similar, with small differences. The structure of GluA2 LBD bound to NO_2W is shown in Figure 6A, and structural statistics are given in Supplemental Table 2. In all cases, the LBD dimer interface, seen in the structure of the tetrameric protein (Sobolevsky et al., 2009), was observed. The dimer interface is essentially the same for each of the agonists bound to the LBD, and it is similar to the dimer interface observed with cyclothiazide derivatives bound (Ptak et al., 2009). FW bound GluA3 is 2.6˚ more open relative to glutamate (3DP6, B protomer, glutamate bound to GluA2 (Ahmed et al., 2009b; Table 4). The structure of the GluA2 LBD bound to FW has been reported previously (Jin et al., 2003) and overall is similar to the GluA3

Molecular Pharmacology Fast Forward. Published on April 4, 2011 as DOI: 10.1124/mol.111.071688
This article has not been copyedited and formatted. The final version may differ from this version.

LBD structure reported here. The FW bound GluA2 structure is 4˚ more open relative to glutamate.

The structures of ClW bound to the LBDs of GluA2 and GluA3 were determined. Despite the somewhat smaller size of the chlorine relative to the nitro moiety, the average lobe opening relative to the most closed glutamate-bound form of GluA3 for ClW bound to GluA2 LBD (4.1˚, 2.4˚, 2.2˚; average 2.9˚ ± 1.0˚) is larger than NO_2W bound to GluA2 LBD, but the distributions overlap. The lobe opening for GluA3 LBD bound to ClW (3.7˚; one copy per asymmetric unit) is within the range observed for GluA2.

Three crystals of NO_2W bound to GluA2 LBD, each with three structures per asymmetric unit, were analyzed. Despite the fact that the nitro substituent of NO_2W is larger than the fluorine of FW, six of the nine structures in the asymmetric unit for NO_2W bound to GluA2 LBD are more closed than observed for FW bound to either GluA2 or GluA3 LBD. In fact, six of the nine structures were more closed than one of the structures of GluA2 bound to glutamate (3DP6, A protomer, 1.75˚). The most striking aspect of the NO_2W structure is the variation observed. The range of lobe opening relative to the most closed glutamate-bound structure is more than 3˚ (0.7 to 3.9˚; average 2.0˚ ± 1.7˚).

D655/S656 peptide conformation: The flipped conformation of the D655/S656 peptide bond (this and all subsequent residues are given in GluA3 numbering; for GluA2, the corresponding peptide bond is D651/S652), which is typically seen in structures with full agonist bound (Armstrong and Gouaux, 2000), allows the formation of two H-bonds across the lobe interface: the carbonyl of S656 (Lobe 2) forms an H-bond with the amide of G453 (Lobe 1) and the carbonyl of D655 forms a water-mediated H-bond with the amide of Y452 (Figure 6E). This conformation has been suggested to relate to modal behaviors; that is, the formation of these hydrogen bonds in individual subunits may stabilize its active form and the combination of those subunits that are or are not H-bonded may result in different modes of activation (Poon et al., 2010). The FW bound GluA3 LBD structure reveals that the D655/S656 peptide bond is in the

Molecular Pharmacology Fast Forward. Published on April 4, 2011 as DOI: 10.1124/mol.111.071688
This article has not been copyedited and formatted. The final version may differ from this version.

flipped conformation (Figure 6B). Although this conformation has not been observed crystallographically for the GluA2 LBD bound to FW, residual dipolar coupling measurements using NMR spectroscopy (Maltsev et al., 2008) suggested that FW-bound GluA2 can also assume a flipped conformation for the D655/S656 peptide bond. In the case of FW bound to GluA3, the lobes are slightly more separated than with glutamate so that neither the water-mediated D655-Y452 H-bond nor the direct H-bond between S656 and G453 is formed. Instead, an additional water molecule sits in the pocket forming an H-bonding network that includes the backbone carbonyl of S656 and the backbone amides of G453 and Y452 (Figure 6B). This may result in additional stability in this partially open form of the LBD.

The GluA3 LBD structure bound to ClW exhibits several interesting features (Figure 6C, D). Unlike other structures that are not fully closed but similar to the FW GluA3 LBD structure, the D655/S656 peptide bond is in the flipped conformation. The question then is whether the H-bonds typical of the flipped conformation are formed. The carbonyl of D655 probably does not participate in an H-bond with the amide of Y452, although the water molecule is in the appropriate position. However, an acetate molecule is present in the cleft that forms an interlobe H-bond with the backbone carbonyls of D655 and K451 (Figure 6C). Although, the carbonyl of S656 is not sufficiently close to the amide of G453 to make a direct H-bond, there exists an H-bonding network involving three water molecules that joins the carbonyl of S656 to the amides of both Y452 and G453 (Figure 6C). This seems to suggest that a semi-stable partially open, flipped conformation exists. In contrast, all three structures of GluA2 LBD bound to ClW are in the unflipped conformation; however, in two of the three structures, the three water molecules are in similar positions (Figure 6D). The sidechain of S656 (S652 in GluA2) is rotated to form a water-mediated H-bond with G453. In all three copies, both the backbone carbonyl and the sidechain of D655 interact with K660 (Figure 6D).

The nine structures of NO_2W bound to GluA2 show considerable variability. In the most closed structure, the D655/S656 peptide bond is in the flipped conformation (Figure 6E), with

Molecular Pharmacology Fast Forward. Published on April 4, 2011 as DOI: 10.1124/mol.111.071688
This article has not been copyedited and formatted. The final version may differ from this version.

the H-bonds to Y452 and G453 formed as observed for full agonists. For the remainder, the bond is not flipped, and in some cases, two conformations of the sidechain of D655 are apparent (Figure 6F). The sidechain of D655 can form a salt bridge with the sidechain of K660. This is seen in the conformer with the flipped peptide bond, but only one of the two conformations of the D655 sidechain can form this salt bridge in the two unflipped structures. In the case of the unflipped structure, the sidechain of K660 can interact with both the sidechain and backbone carbonyl of D655 (Figure 6F). However, in the flipped form, the carbonyl of D655 forms an interlobe H-bond with Y452, so that only the D655 sidechain is available for interaction with K660. In addition, the nitro group of NO_2W contributes interactions that may stabilize the closed lobe conformation; NO_2W can form an H-bond with the sidechain of T690 and the sidechain hydroxyl of Y452 (Figure 7A).

Although these structures capture either the flipped or unflipped conformations of D655-S656, it is very likely that both of these states are visited in solution. Based on the structures reported here, it seems the flipped conformation of the D655/S656 peptide can exist in partially closed LBD structures and is stabilized by water molecules occupying the partially open space. NMR results (Maltsev et al., 2008) suggest the GluA2 LBD exhibits an equilibrium between the flipped and unflipped conformations, which means either form could be crystallized. The differences in the flipped region between GluA2 and GluA3 are unlikely to be functional differences but rather both conformations are most likely present in both subtypes.

Met 712 sidechain conformation: M712, located in helix I, has been seen to adopt different conformations depending on the agonist that is bound (Armstrong and Gouaux, 2000; Jin and Gouaux, 2003; Jin et al., 2002). In glutamate-bound and FW-bound GluA2 and GluA3 structures, M712 is in an extended conformation. For NO_2W, comparison of the structure with that of the FW-bound and glutamate-bound GluA2 and GluA3 structures indicates that the larger size of NO_2W is accommodated by a change in the rotameric state of M712 at the β carbon (Figure 7B) and the exclusion of one water molecule (relative to the ClW-bound form) from the

Molecular Pharmacology Fast Forward. Published on April 4, 2011 as DOI: 10.1124/mol.111.071688
This article has not been copyedited and formatted. The final version may differ from this version.

binding pocket (Figure 7C). This places the sidechain in a position that is intermediate between the glutamate-bound form and the form reported previously for BrW and IW (Jin and Gouaux, 2003).

The rotamer of the sidechain of M712 in the ClW bound GluA3 LBD structure is similar to willardiine partial agonists such as BrW and IW. However, in the structure of GluA2 bound to ClW, two of the protomers have a conformation of M712 similar to that of the NO_2W structure and one has density corresponding to both the NO_2W conformation and to the conformation seen with ClW bound to GluA3. As noted above, for ClW, the rotation of the sidechain allows an additional water molecule to enter the binding pocket to interact with the sidechain hydroxyls of Y407 and Y736 (Figure 7C).

Summary. Although the overall structures of the GluA2 and GluA3 LBD are similar for all agonists tested, variability in lobe closure, the state of the peptide flip region, and some side chain rotamers can vary. In addition, NO_2W makes additional contacts that are not observed in other willardiines. These differences may be associated with the functional differences observed in single channel recording.

Discussion

Efficacy of partial agonists

Although recognizing that the lobe closure observed in a crystal may or may not reflect the frequency and extent of lobe closure in an intact receptor, Jin et al (2003) postulated that partial agonism arose from partial lobe closure and efficacy was dependent on the degree of closure. While consistent with the initial crystal structures, more recent work has supported a model in which the stability of full lobe closure determines efficacy (Robert et al., 2005; Zhang et al., 2008a), such that partial closures likely represent intermediate states of low energy in the crystal. The evidence includes a demonstration that partial agonists can exist in a wide range of lobe orientations (Maltsev et al., 2008) that are in equilibrium (Ahmed et al., 2009a; Fenwick

Molecular Pharmacology Fast Forward. Published on April 4, 2011 as DOI: 10.1124/mol.111.071688
This article has not been copyedited and formatted. The final version may differ from this version.

and Oswald, 2008; Maltsev et al., 2008), and that even the lowest efficacy agonists can access a fully closed state (Ahmed et al., in preparation). The crystal structures presented here show that FW-, ClW- and NO_2W-bound LBD access a range of lobe orientations, some of which are fully closed. All structures show multiple side chain orientations near the lobe interface. While multiple sidechain conformations do not directly imply multiple lobe orientations, they suggest the possibility of dynamics near the lobe interface. The sidechain of D655 can make a salt bridge with K660, and the presence or absence of this salt bridge may influence the orientation of the D655/S656 bond and interlobe H-bonding (Holley et al., submitted). These results suggest that partial agonists exist in a range of lobe orientations and the differences in the population of conductance levels are less likely to be associated with a fixed degree of lobe closure. The question is how often these states are visited for each agonist. The fact that GluA2 can be crystallized in the fully closed state when bound to NO_2W may suggest that this state is of low energy. Why then is the efficacy of FW, albeit to a small degree, greater than NO_2W, while the single channel open probabilities are very similar? There are three potential structural differences between the bound forms of FW and NO_2W, including (1) the orientation of M712, (2) additional interactions with Lobe 2 through the nitro group in NO_2W, and (3) possible differences in H-bonding across the lobe interface.

Considering the orientation of M712, the rotameric state in both the ClW and NO_2W structures of GluA2 differs from previous structures (Jin and Gouaux, 2003). Although the significance of this change in rotameric state is difficult to assess, M712 is part of helix I, which undergoes a bending motion when bound to weak partial agonists, such as IW (Fenwick and Oswald, 2008). At the other end of helix I, a disulfide bond connects helix I to the C-terminal portion of the LBD, which in the intact protein is the beginning of the linker to the M4 helix. The M4 helix of one subunit is associated with the ion channel gating region of an adjacent subunit (Sobolevsky et al., 2009) and this slight change in M712 could alter gating kinetics. In fact, mutations in the M4 segment of NMDA receptors alter function (Ren et al., 2003).

Molecular Pharmacology Fast Forward. Published on April 4, 2011 as DOI: 10.1124/mol.111.071688
This article has not been copyedited and formatted. The final version may differ from this version.

With residual dipolar coupling (RDC) measurements using NMR spectroscopy, Maltsev et al. (2008) estimated that the proportion of the flipped conformation of the D655/S656 peptide bond varies with agonist: 0.54, 0.44, 0.46, 0.45, 0.28, and 0.29 for HW, FW, ClW, BrW, IW, and NO_2W, respectively. This would suggest that the D655/S656 bond is in a position to form H-bonds more often for FW and ClW than NO_2W; however, as demonstrated by the GluA3 structures bound to FW and ClW, the flipped peptide bond does not always correspond to a fully closed lobe. The additional contacts made by NO_2W in Lobe 2 (H-bonding to T690 and Y452) may stabilize lobe closure and compensate for the lower propensity to form a flipped conformation.

Modal activation and the peptide flip conformation

Modal activation of glutamate receptors has been reported for NMDA receptors (Popescu and Auerbach, 2003; Zhang et al., 2008b), GluA3 (Poon et al., 2010), and GluA1, GluA2, and GluA4 (Prieto and Wollmuth, 2010). Prieto and Wollmuth (2010) demonstrated a lack of bionomial gating at subsaturating concentrations of glutamate in 200 ms records from outside-out patches, suggesting two gating modes. A cooperative interaction between subunits was postulated to change the affinity at lower concentrations of glutamate. In longer recordings, Poon et al. (2010) detected five distinct gating modes that were observed in both glutamate and FW. Although higher modes were more likely to be observed at higher concentrations, all modes were observed at all concentrations tested. Like glutamate and FW, activation of the channel by NO_2W and ClW exhibits five modes of activation (VL, L, M, H, and VH; Figure 4). It is currently not possible to determine if the two modes observed by Prieto and Wollmuth (2010) correspond to those described here. The difference may have arisen because the records reported here were obtained in cell-attached patch recordings and were considerably longer than those described by Prieto and Wollmuth (2010).

We previously postulated (Poon et al., 2010) that modal behavior could arise from locking a specified number of LBDs in the tetramer closed as a result of the flipping of the

Molecular Pharmacology Fast Forward. Published on April 4, 2011 as DOI: 10.1124/mol.111.071688
This article has not been copyedited and formatted. The final version may differ from this version.

D655/S656 peptide bond. When full agonists are bound, the D655/S656 peptide bond flip results in the formation of two H-bonds between the carbonyl of S656 (Lobe 2) and the amide of G453 (Lobe 1), and between the carbonyl of D655 and the amide of Y452 through a water molecule. The fully closed, H-bonding pattern exists on the timescale of approximately 100 ms (Fenwick and Oswald, 2010), which is the timescale of modal gating. The number and arrangement of subunits bound to agonist and in the H-bond locked state could determine the mode. As described previously (Poon et al., 2010), the VH mode might be generated by full occupancy and 3-4 H-bonded subunits, and the lower modes would have progressively fewer H-bonds and a tendency toward lower occupation.

FW and ClW bound to GluA3 LBD show a variation on this H-bonding pattern. The peptide bond is flipped in the context of lobes that are slightly more open (~3˚ relative to the glutamate structure), making the H-bonds difficult to form. However, additional water molecules enter the cleft (in one case, an acetate molecule) and mediate the H-bonds between the two lobes. These hybrid H-bonded conformations have not been previously reported and may result in subtle functional effects. One possible outcome is the alternate kinetics observed with ClW in H mode. Assuming the modes are set by the occupancy and H-bonding state (Poon et al., 2010), this hybrid H-bonding state increases the number of possibilities. If the hybrid H-bonding state has the same stability as the fully closed pattern but actually is a conformation that does not permit channel activation, then the H and VH modes that have extremely low probability for the largest conductance state may arise from a fully occupied tetramer with two to three subunits in the standard H-bonding conformation and one or two in the hybrid conformation.

Dwell time variation between agonists

In the VH mode, NO_2W exhibits relatively long channel lifetimes and the overall efficacy is slightly better than ClW. The size of the nitro group is larger than the chloro substituent, but the lobes are, on average, more closed for NO_2W than ClW. The fraction of bound NO_2W in the flipped conformation calculated from RDC measurements suggest NO_2W

Molecular Pharmacology Fast Forward. Published on April 4, 2011 as DOI: 10.1124/mol.111.071688
This article has not been copyedited and formatted. The final version may differ from this version.

was 0.29 (similar to another low efficacy partial agonist, iodowillardiine); whereas, the fractions for ClW and FW were 0.46 and 0.44, respectively (Maltsev et al., 2008). However, the additional contacts of NO_2W to the sidechains of T690 and Y452 may help stabilize the fully closed state and contribute to longer openings in each conductance level. These interactions are not present in the other willardiine partial agonists and may compensate for the decreased population of the flipped conformation.

Conclusions

The structures of the willardiines bound to GluA2 and GluA3 LBD suggest full lobe closures are possible, particularly with NO_2W. Structures of kainate bound to the LBD of a kainate receptor reveal 3° less closure than glutamate and yet kainate is a full agonist at kainate receptors (Mayer, 2005), further implying crystal structures represent a subset of accessible conformational states. Partial agonists at NMDA receptors exhibit full lobe closures (Inanobe et al., 2005; Kussius et al., 2010). Although NMDA receptors have very different activation kinetics (slow activation, long openings) compared to AMPA receptors, the mechanism leading to a gating event may be conserved for all subtypes of glutamate receptors. Taken together with our previous results (Poon et al., 2010), these findings imply that agonist efficacy may be dependent upon the relative fraction of time spent in an ensemble of conformations that include fully open, fully closed, and intermediate degrees of closure. The stability of each conformer is in turn determined by multiple interlobe contacts that can differ between different agonists.

Acknowledgements

The authors would like to thank Dr. Sandra Holley (UCLA), Dr. Jayasri Srinivasan (Cornell), Dr. Gregory Weiland (Cornell), Bethsabe Romero, Dr. Fred Sachs (SUNY Buffalo), Dr. Anthony Auerbach (SUNY Buffalo) and Chris Nicolai (SUNY Buffalo) for helpful advice, technical support and discussions.

Molecular Pharmacology Fast Forward. Published on April 4, 2011 as DOI: 10.1124/mol.111.071688
This article has not been copyedited and formatted. The final version may differ from this version.

Authorship contributions

Participated in research design: Poon, Ahmed, Nowak, and Oswald

Conducted single channel recording experiments: Poon and Nowak

Analyzed single channel recording experiments: Poon, Nowak and Oswald

Purified protein, prepared crystals, and collected X-ray data: Ahmed

Analyzed X-ray data: Ahmed and Oswald

Wrote or contributed to writing paper: Poon, Ahmed, Nowak, and Oswald

Other: Oswald, Nowak, and Poon acquired funding for the research.

Molecular Pharmacology Fast Forward. Published on April 4, 2011 as DOI: 10.1124/mol.111.071688
This article has not been copyedited and formatted. The final version may differ from this version.

References

Abele R, Keinanen K and Madden DR (2000) Agonist-induced isomerization in a glutamate receptor ligand-binding domain. A kinetic and mutagenetic analysis. *J Biol Chem* **275**:21355-21363.

Adams PD, Grosse-Kunstleve RW, Hung LW, Ioerger TR, McCoy AJ, Moriarty NW, Read RJ, Sacchettini JC, Sauter NK and Terwilliger TC (2002) PHENIX: building new software for automated crystallographic structure determination. *Acta Crystallogr D Biol Crystallogr* **58**:1948-1954.

Ahmed A, Thompson M, Fenwick M, Romero B, Loh A, Jane D, Sondermann H and Oswald R (2009a) Mechanisms of antagonism of the GluR2 AMPA receptor: Structure and dynamics of the complex of two willardiine antagonists with the glutamate binding domain. *Biochemistry* **48**:3894-3903.

Ahmed AH, Wang Q, Sondermann H and Oswald RE (2009b) Structure of the S1S2 glutamate binding domain of GluR3. *Proteins: Structure, Function, and Bioinformatics* **75**:628-637.

Armstrong N and Gouaux E (2000) Mechanisms for activation and antagonism of an AMPA-sensitive glutamate receptor: crystal structures of the GluR2 ligand binding core. *Neuron* **28**:165-181.

Banke TG and Traynelis SF (2003) Activation of NR1/NR2B NMDA receptors. *Nat Neurosci* **6**:144-152.

Cheng Q, Du M, Ramanoudjame G and Jayaraman V (2005) Evolution of glutamate interactions during binding to a glutamate receptor. *Nature chemical biology* **1**:329-332.

Citri A and Malenka RC (2008) Synaptic plasticity: multiple forms, functions, and mechanisms. *Neuropsychopharmacology* **33**:18-41.

Collaborative_Computational_Project (1994) The CCP4 suite: programs for protein crystallography. *Acta Crystallogr D Biol Crystallogr* **50**:760-763.

Derkach VA, Oh MC, Guire ES and Soderling TR (2007) Regulatory mechanisms of AMPA receptors in synaptic plasticity. *Nat Rev Neurosci* **8**:101-113.

Dingledine R, Borges K, Bowie D and Traynelis S (1999) The glutamate receptor ion channels. *Pharmacol Rev* **51**:7-61.

Emsley P and Cowtan K (2004) Coot: model-building tools for molecular graphics. *Acta Crystallogr D Biol Crystallogr* **60**:2126-2132.

Fenwick MK and Oswald RE (2008) NMR spectroscopy of the ligand-binding core of ionotropic glutamate receptor 2 bound to 5-substituted willardiine partial agonists. *J Mol Biol* **378**:673-685.

Fenwick MK and Oswald RE (2010) On the mechanisms of alpha-amino-3-hydroxy-5-methylisoxazole-4-propionic acid (AMPA) receptor binding to glutamate and kainate. *J Biol Chem* **285**:12334-12343.

Hayward S and Lee RA (2002) Improvements in the analysis of domain motions in proteins from conformational change: DynDom version 1.50. *J Mol Graph Model* **21**:181-183.

Heath PR and Shaw PJ (2002) Update on the glutamatergic neurotransmitter system and the role of excitotoxicity in amyotrophic lateral sclerosis. *Muscle Nerve* **26**:438-458.

Hollmann M and Heinemann S (1994) Cloned glutamate receptors. *Annu Rev Neurosci* **17**:31-108.

Hynd MR, Scott HL and Dodd PR (2004) Glutamate-mediated excitotoxicity and neurodegeneration in Alzheimer's disease. *Neurochem Int* **45**:583-595.

Inanobe A, Furukawa H and Gouaux E (2005) Mechanism of partial agonist action at the NR1 subunit of NMDA receptors. *Neuron* **47**:71-84.

Jin R, Banke TG, Mayer ML, Traynelis SF and Gouaux E (2003) Structural basis for partial agonist action at ionotropic glutamate receptors. *Nat Neurosci* **6**:803-810.

Jin R and Gouaux E (2003) Probing the function, conformational plasticity, and dimer-dimer contacts of the GluR2 ligand-binding core: Studies of 5-substituted willardiines and GluR2 S1S2 in the crystal. *Biochemistry* **42**:5201-5213.

Jin R, Horning M, Mayer ML and Gouaux E (2002) Mechanism of activation and selectivity in a ligand-gated ion channel: structural and functional studies of GluR2 and quisqualate. *Biochemistry* **41**:15635-15643.

Kussius CL, Popescu AM and Popescu GK (2010) Agonist-specific gating of NMDA receptors. *Channels (Austin)* **4**:78-82.

Kussius CL and Popescu GK (2009) Kinetic basis of partial agonism at NMDA receptors. *Nat Neurosci* **12**:1114-1120.

Liu SJ and Zukin RS (2007) Ca2+-permeable AMPA receptors in synaptic plasticity and neuronal death. *Trends Neurosci* **30**:126-134.

Magleby KL and Pallotta BS (1983) Burst kinetics of single calcium-activated potassium channels in cultured rat muscle. *J Physiol* **344**:605-623.

Maltsev AS, Ahmed AH, Fenwick MK, Jane DE and Oswald RE (2008) Mechanism of partial agonism at the GluR2 AMPA receptor: Measurements of lobe orientation in solution. *Biochemistry* **47**:10600-10610.

Mayer ML (2005) Crystal structures of the GluR5 and GluR6 ligand binding cores: Molecular mechanisms underlying kainate receptor selectivity. *Neuron* **45**:539-552.

Otwinowski Z and Minor W (1997) Processing of X-ray diffraction data collected in oscillation mode, in *Methods in Enzymology, Vol 276, Macromolecular Crystallography, part A* (Carter CW and Sweet RM eds) pp 307-326, Academic Press, New York.

Patneau DK, Mayer ML, Jane DE and Watkins JC (1992) Activation and desensitization of AMPA/kainate receptors by novel derivatives of willardiine. *J Neurosci* **12**:595-606.

Pelleg D and Moore AW (2000) *X-means: extending K-menas with efficient estimation of the number of clusters.* Morgan Kaufmann Publishers, San Francisco, CA.

Poon K, Nowak LM and Oswald RE (2010) Characterizing single-channel behavior of GluA3 receptors. *Biophys J* **99**:1437-1446.

Popescu G and Auerbach A (2003) Modal gating of NMDA receptors and the shape of their synaptic response. *Nat Neurosci* **6**:476-483.

Prieto ML and Wollmuth LP (2010) Gating modes in AMPA receptors. *J Neurosci* **30**:4449-4459.

Ptak CP, Ahmed AH and Oswald RE (2009) Probing the allosteric modulator binding site of GluR2 with thiazide derivatives. *Biochemistry* **48**:8594-8602.

Qin F, Auerbach A and Sachs F (1996) Estimating single-channel kinetic parameters from idealized patch-clamp data containing missed events. *Biophys J* **70**:264-280.

Ren H, Honse Y, Karp BJ, Lipsky RH and Peoples RW (2003) A site in the fourth membrane-associated domain of the N-methyl-D-aspartate receptor regulates desensitization and ion channel gating. *J Biol Chem* **278**:276-283.

Robert A, Armstrong N, Gouaux JE and Howe JR (2005) AMPA receptor binding cleft mutations that alter affinity, efficacy, and recovery from desensitization. *J Neurosci* **25**:3752-3762.

Rosenmund C, Stern-Bach Y and Stevens CF (1998) The tetrameric structure of a glutamate receptor channel. *Science* **280**:1596-1599.

Silberberg SD, Lagrutta A, Adelman JP and Magleby KL (1996) Wanderlust kinetics and variable $Ca(^{2+})$-sensitivity of dSlo, a large conductance $CA(^{2+})$-activated K^+ channel, expressed in oocytes. *Biophys J* **71**:2640-2651.

Smith TC and Howe JR (2000) Concentration-dependent substate behavior of native AMPA receptors. *Nat Neurosci* **3**:992-997.

Sobolevsky AI, Rosconi MP and Gouaux E (2009) X-ray structure, symmetry and mechanism of an AMPA-subtype glutamate receptor. *Nature* **462**:745-756.

Traynelis SF, Wollmuth LP, McBain CJ, Menniti FS, Vance KM, Ogden KK, Hansen KB, Yuan H, Myers SJ, Dingledine R and Sibley D (2010) Glutamate receptor ion channels: structure, regulation, and function. *Pharmacol Rev* **62**:405-496.

Weston MC, Gertler C, Mayer ML and Rosenmund C (2006) Interdomain interactions in AMPA and kainate receptors regulate affinity for glutamate. *J Neurosci* **26**:7650-7658.

Zhang W, Cho Y, Lolis E and Howe JR (2008a) Structural and single-channel results indicate that the rates of ligand binding domain closing and opening directly impact AMPA receptor gating. *J Neurosci* **28**:932-943.

Zhang W, Howe JR and Popescu GK (2008b) Distinct gating modes determine the biphasic relaxation of NMDA receptor currents. *Nat Neurosci* **11**:1373-1375.

Molecular Pharmacology Fast Forward. Published on April 4, 2011 as DOI: 10.1124/mol.111.071688
This article has not been copyedited and formatted. The final version may differ from this version.

Footnotes

This work was supported by a grant from the National Institutes of Health [R01 NS049223]. Kinning Poon was supported by a National Institutes of Health Ruth L. Kirschstein National Research Service Award [1F31NS063518].

[1]Dual PIs.

Please address reprint requests to:

Robert E. Oswald

Department of Molecular Medicine

Cornell University

Ithaca, NY 14853

reo1@cornell.edu

Molecular Pharmacology Fast Forward. Published on April 4, 2011 as DOI: 10.1124/mol.111.071688
This article has not been copyedited and formatted. The final version may differ from this version.

Legends to Figures

Figure 1. (A) The final kinetic model used to analyze the single channel data. The notation for the equilibrium association constants is: $K_{C21} = k_{C2\to C1}/k_{C1\to C2}$, $K_{O12a} = k_{O1a\to O2a}/k_{O2a\to O1a}$, $K_{O1ab} = k_{O1a\to O1b}/k_{O1b\to O1a}$, etc. (B) Transition matrices showing the percentage of transitions between conductance levels (*i.e.*, transitions between sublevels). Transitions between nonadjacent states are rare compared to transitions between adjacent states. These data are used to constrain the final kinetic model such that only transitions between adjacent states are included (C to O_2, C to O_3 and O_1 to O_3 are not included in the model).

Figure 2. (A) A 500 ms representative segment of a GluA3 channel activated by 100 μM NO_2W opens to three different conductance levels. (B, C) Amplitude histograms and Gaussian fits for an entire record obtained with 500 μM NO_2W at 100 mV (B) and 500 μM ClW at 80 mV (C). For both the NO_2W and ClW records shown, the channel exhibited VH mode. The idealization was done using a deadtime of 200 μs (see Methods).

Figure 3. Dwell time histograms for the same records used to generate Figures 2B and C. MIL (Qin et al., 1996) was used to fit the data to the model shown in Figure 1A.

Figure 4. (A) Representative 500 ms segments of single channel records showing modal behaviors for 50 μM ClW (VL), 100 μM ClW (L, M, H), 500 μM ClW (VH), and 50 μM NO_2W (VL, L), 100 μM NO_2W (M, H), 500 μM NO_2W (VH). The traces are additionally filtered at 1 kHz for display purposes. (B) Segment of a record with 100 μM ClW as the agonist showing the changes in P_o as a function of time (the segments of closed time greater than t_{crit} are removed from the record). (C) The same record as (B) is shown with mode classification. Note that, as described by Poon et al. (2010), the transitions are most likely to occur between adjacent modes (*e.g.*, VL to L, H to M, *etc*.)

Figure 5. (A) The efficacy factor (p) was calculated as described in Poon et al. (2010) based on the amplitude histograms for records separated into specific modes. The concentrations used

Molecular Pharmacology Fast Forward. Published on April 4, 2011 as DOI: 10.1124/mol.111.071688
This article has not been copyedited and formatted. The final version may differ from this version.

ranged from 50 to 1000 μM for ClW and NO_2W. The values for FW and glutamate were taken from Poon et al. (2010).The dotted line is to the alternative kinetic behavior exhibited at lower concentrations of ClW. The efficacy factor is synonymous with the probability of success in a bionomial distribution. The higher the value, the more likely a gate will be open. (B) Example of the alternate kinetic behavior exhibited when ClW activates the channel.

Figure 6. (A) GluA2 LBD bound to NO_2W ($P2_12_12$, R = 18.9, R_{free} = 22.2, 1.78 Å resolution). The N-terminal portion of the LBD is shown in cyan and the segment between M3 and M4 is shown in green. (B) FW bound to GluA3 LBD ($P222_1$, R = 19.6, R_{free} = 25.5, 2.85 Å resolution). The D655/S656 is in the flipped conformation; however, and two waters mediate a hydrogen bonding network involving the backbone carbonyl of S656 and the backbone amides of G453 and Y452. (C) ClW bound to GluA3 LBD ($P222_1$, R = 22.3, R_{free} = 27.8, 2.4 Å resolution). The D655/S656 is in the flipped conformation; however, an acetate molecule is present which forms an interlobe H-bond with the backbone carbonyls of D655 and K451, as well as three water molecules that join the carbonyl of S656 to the amides of both Y452 and G453. The acetate is a component of the crystallization buffer. (D) ClW bound to GluA2 LBD ($P22_12_1$, R = 18.2, R_{free} = 20.3, 1.7 Å resolution). The D655(D651)/S656(S652) is in the unflipped conformation. (E) NO_2W bound to GluA2 LBD. The D655(D651)/S656(S652) is in the appropriate position to form hydrogen bonds to G453(G451) and Y452(Y450). (F) NO_2W bound to GluA2 LBD. The D655(D651)/S656(S652) is in the unflipped conformation. For both ClW and NO_2W, the sidechain of D655(D651) forms a salt bridge with K660(K656). For all GluA2 structures, residue numbering is given as that for GluA3, with the GluA2 numbering in parenthesis.

Figure 7. (A) The nitro group of NO_2W bound to GluA2 contributes to stability by making additional H-bonds to T686 and Y450 (GluA2 numbering; T690 and Y452 GluA3 equivalent). Residue numbering is that for GluA3, with the GluA2 numbering in parenthesis. (B) The sidechain of M712 is in an extended state when bound to FW (cyan). There is a rotomeric change at the β carbon when bound to NO_2W (green). The rotameric change is most dramatic

Molecular Pharmacology Fast Forward. Published on April 4, 2011 as DOI: 10.1124/mol.111.071688
This article has not been copyedited and formatted. The final version may differ from this version.

with ClW bound (magenta). (C) The change in the rotameric state of M712 when ClW is bound makes room for binding of an additional water molecule.

Molecular Pharmacology Fast Forward. Published on April 4, 2011 as DOI: 10.1124/mol.111.071688
This article has not been copyedited and formatted. The final version may differ from this version.

Table 1

Average Population of Each Conductance Level in VH Mode

Shown is the averaged probability of the GluA3 channel visiting each conductance level in the VH mode for glutamate, FW, NO_2W and ClW (n=3 for each agonist). The last row ($\Sigma P\gamma$) reports the sum of the P for each row multiplied by the conductance normalized to the value for glutamate. The conductances for glutamate and FW were taken from Poon et al. (2010).

	5 mM glutamate	200 µM FW	500 µM NO_2W	500 µM ClW
P_C	6% ± 3	9% ± 1	12 ± 3%	13 ± 2%
P_{O1}	6% ± 3	22% ± 5	37 ± 5%	31 ± 3%
P_{O2}	51% ± 6	47% ± 2	33 ± 4%	42 ± 3%
P_{O3}	36% ± 12	22% ± 7	17 ± 2%	14 ± 4%
$\Sigma P\gamma$	1.0	0.81	0.79	0.73

Molecular Pharmacology Fast Forward. Published on April 4, 2011 as DOI: 10.1124/mol.111.071688
This article has not been copyedited and formatted. The final version may differ from this version.

Table 2

Equilibrium Constants for Modes Derived from Single Channel Records

Equilibrium association constants were determined using the model defined in Figure 1 for NO_2W and ClW as the agonist. The equilibrium constants were averaged across all concentrations in a given mode. All constants are unitless, and errors are given as SEM. The number of patches analyzed is given in parenthesis after the mode.

NO_2W

Mode	K_{C32}	K_{C21}	K_{C1O}	K_{O1ab}	K_{O12a}	K_{O2ab}	K_{O23a}	K_{O3ab}
VH (12)	3.5 ± 0.8	1.9 ± 0.3	3.7 ± 0.6	0.40 ± 0.07	1.2 ± 0.1	0.42 ± 0.08	0.44 ± 0.07	0.55 ± 0.10
H (15)	4.8 ± 1.5	1.5 ± 0.2	2.0 ± 0.1	0.31 ± 0.04	0.80 ± 0.04	0.30 ± 0.08	0.30 ± 0.03	0.37 ± 0.04
M (4)	2.3 ± 0.4[1]	1.6 ± 0.3	1.2 ± 0.1	0.18 ± 0.04	0.31 ± 0.05	0.20 ± 0.04	0.18 ± 0.04	0.33 ± 0.02
L (3)	1.8 ± 0.3	1.1 ± 0.1	0.6 ± 0.1	0.55 ± 0.42	0.19 ± 0.04	0.23 ± 0.07	0.16 ± 0.01	0.24 ± 0.02

ClW

Mode	K_{C32}	K_{C21}	K_{C1O}	K_{O1ab}	K_{O12a}	K_{O2ab}	K_{O23a}	K_{O3ab}
VH (11)	2.0 ± 0.3	2.3 ± 0.2	3.7 ± 0.5	0.54 ± 0.27	2.3 ± 0.8	0.17 ± 0.03	0.29 ± 0.05	0.30 ± 0.06
H (12)	5.9 ± 2.6	1.7 ± 0.1	2.1 ± 0.1	0.18 ± 0.03	0.62 ± 0.08	0.21 ± 0.04	0.19 ± 0.04	0.40 ± 0.09
M (2)	2.3 ± 0.3	1.2 ± 0.1	1.2 ± 0.1	0.17 ± 0.02	0.40 ± 0.09	0.13 ± 0.02	0.21 ± 0.06	0.31 ± 0.03
L (4)	1.6 ± 0.2	0.92 ± 0.07	1.0 ± 0.1	0.17 ± 0.03	0.26 ± 0.03	0.14 ± 0.02	0.12 ± 0.02	0.34 ± 0.03
VL (4)	2.3 ± 0.6	1.0 ± 0.1	0.34 ± 0.09	0.19 ± 0.03	0.26 ± 0.11	0.10 ± 0.04	0.09 ± 0.03	0.33 ± 0.06

[1]One outlier with a K_{C32} of 36 was removed as it was based on a limited number of events.

Molecular Pharmacology Fast Forward. Published on April 4, 2011 as DOI: 10.1124/mol.111.071688
This article has not been copyedited and formatted. The final version may differ from this version.

Table 3

Dwell Times for Modes Derived from Single Channel Records

Dwell times (ms) were determined using the model defined in Figure 1 for NO_2W and ClW as the agonist. The dwell times were averaged across all concentrations in a given mode. The entries in bold are significantly different ($p < .05$) between NO_2W- and ClW-activated channels. For example, the τ_{O3b} for NO_2W is significantly longer than the τ_{O3b} for ClW. The number of patches analyzed is given in parenthesis after the mode.

NO_2W

Mode	τ_{C1}	τ_{C2}	τ_{C3}	τ_{O1a}	τ_{O1b}	τ_{O2a}	τ_{O2b}	τ_{O3a}	τ_{O3b}
VH (12)	1.5 ± 0.2	6.7 ± 1.0	27 ± 3	2.1 ± 0.3	**9.3 ± 2.1**	2.1 ± 0.3	**13 ±4**	2.3 ± 0.3	**16 ± 3**
H (15)	1.6 ± 0.2	7.6 ± 0.8	33 ± 4	1.5 ± 0.1	5.8 ± 0.6	1.5 ± 0.2	5.8 ± 1.4	1.3 ± 0.1	6.2 ± 0.5
M (4)	1.5 ± 0.2	7.0 ± 0.9	31 ± 7	2.1 ± 0.7	6.0 ± 1.8	1.1 ± 0.2	3.9 ± 1	0.9 ± 0.03	4.7 ± 0.9
L (3)	2.2 ± 0.2	9.4 ± 0.3	36 ± 5	1.3 ± 0.2	5.9 ± 2.2	0.8 ± 0.1	3.3 ± 0.7	0.8 ± 0.1	4.3 ± 1.4

ClW

Mode	τ_{C1}	τ_{C2}	τ_{C3}	τ_{O1a}	τ_{O1b}	τ_{O2a}	τ_{O2b}	τ_{O3a}	τ_{O3b}
VH (11)	0.9 ± 0.1	4.1± 0.3	30 ± 5	1.1 ± 0.2	**4.5 ± 0.7**	1.8 ± 0.2	**5.1 ± 0.6**	1.6 ± 0.2	**7.2 ± 1.0**
H (12)	1.3 ± 0.2	5.5 ± 0.7	32 ± 5	1.6 ± 0.2	5.5 ± 1.0	1.5 ± 0.2	5.9 ± 1.4	1.0 ± 0.1	5.6 ± 1.0
M (2)	1.2 ± 0.3	6.0± 0.04	27 ± 5	1.0 ± 0.2	3.2 ± 0.6	0.8 ± 0.1	2.6 ± 0.6	0.9 ± 0.1	4.5 ± 1.0
L (4)	1.4 ± 0.2	7.1 ± 0.8	35 ± 6	1.3 ± 0.1	4.2 ± 0.2	1.2 ± 0.2	3.9 ± 0.6	1.0 ± 0.1	4.6 ± 0.2
VL (4)	1.6 ± 0.3	6.9 ± 1.1	23 ± 5	0.7 ± 0.2	2.4 ± 0.6	0.7 ± 0.1	2.9 ± 0.5	0.9 ± 0.2	5.5 ± 1.5

Molecular Pharmacology Fast Forward. Published on April 4, 2011 as DOI: 10.1124/mol.111.071688
This article has not been copyedited and formatted. The final version may differ from this version.

Table 4

Summary of structures of the LBD of GluA2 and GluA3.

The degree of lobe opening was determined using the Domain Select function in DynDom (Hayward and Lee, 2002). The reference structure is the B protomer of the glutamate-bound form of $GluA2_o$ (3DP6; Ahmed et al., 2009b). Lobe opening is shown relative to the reference structure for each protomer. Either one or three protomers were observed in the asymmetric unit. Three crystals of GluA2 bound to NO_2W were analyzed with three protomers each. In the cases where more than one structure was obtained, the average and standard deviation is given followed by the range of lobe openings. The flipped vs. unflipped conformation of the D655/S656 (GluA3 numbering) peptide bond is relative to the apo form as described by Armstrong and Gouaux (Armstrong and Gouaux, 2000) and is indicated in the column labeled "peptide." The notation, "f" or "u", indicates flipped or unflipped and the number before the letter indicates the number of protomers in that conformation.

GluA2					**GluA3**			
Agonist	PDB	peptide	lobe opening		Agonist	PDB	peptide	lobe opening
Glu[a]	3DP6	3f	0.8˚ ± 0.8˚	(0˚-1.7˚)	Glu[a]	3DLN	1f	0.8˚
FW[b]	1MY4	1u		4˚	FW	*	1f	2.6˚
ClW	*	3u	2.9˚ ± 1.0˚	(2.2˚-4.1˚)	ClW	*	1f	3.7˚
NO_2W	*	8u, 1f	1.9˚ ± 1.2˚	(0.7˚-3.9˚)				

[a]Ahmed et al., 2009b

[b]Jin and Gouaux, 2003

*Structures to be submitted to the Protein Data Bank before publication

Figure 1

A

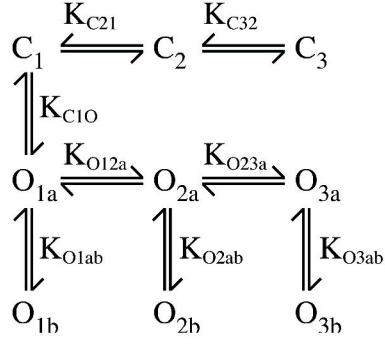

B

500 μM ClW	C	O_1	O_2	O_3
C	-	8.95	1.13	0.04
O_1	8.70	-	25.20	0.53
O_2	1.37	24.81	-	14.36
O_3	0.05	0.66	14.21	-

500 μM NO_2W	C	O_1	O_2	O_3
C	-	7.99	0.41	0.01
O_1	8.22	-	25.14	1.24
O_2	0.19	25.64	-	14.96
O_3	0.00	0.97	15.23	-

Figure 2

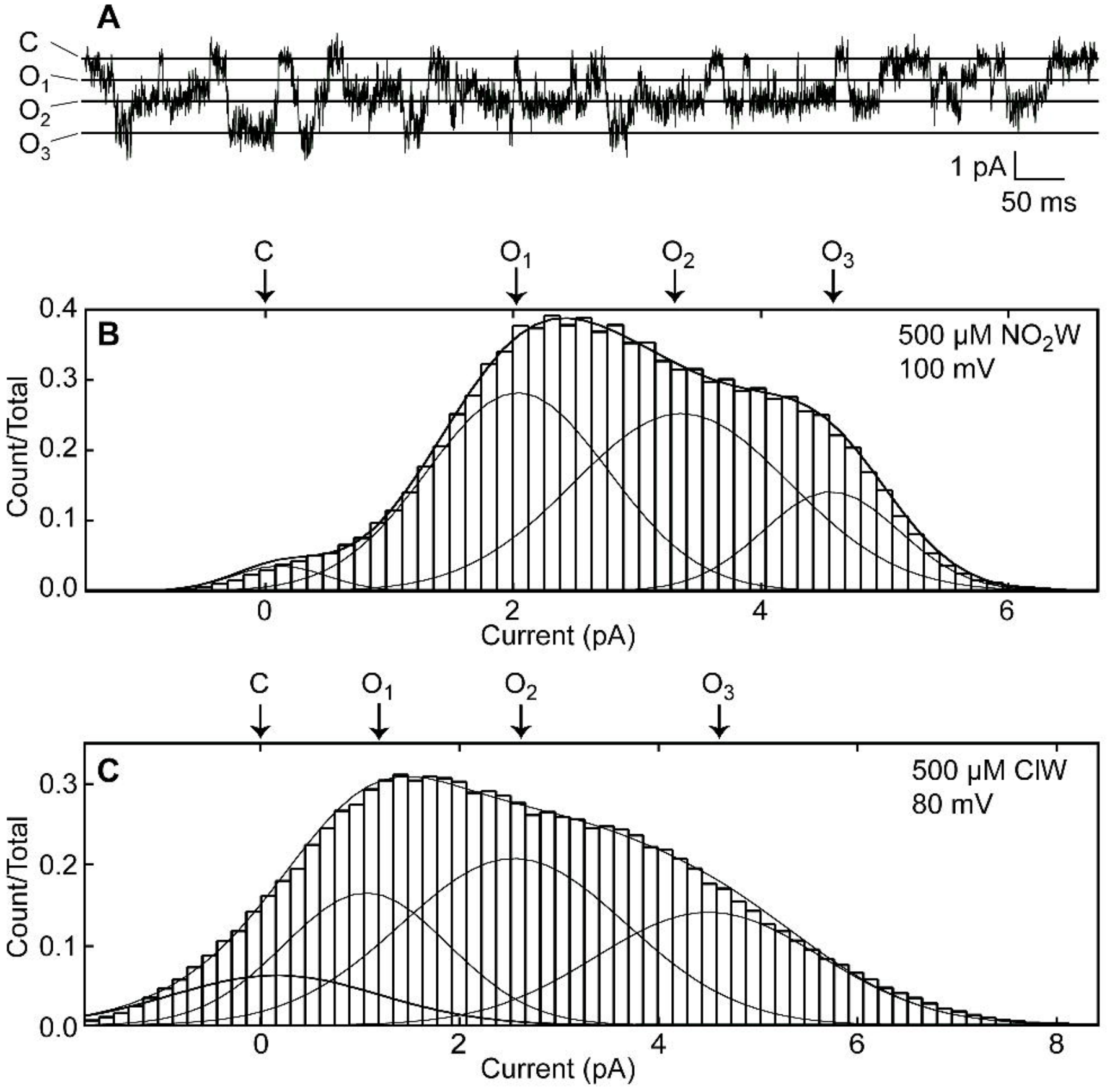
A
C
O1
O2
O3
1 pA
50 ms
B
C
O1
O2
O3
500 μM NO2W
100 mV
Count/Total
Current (pA)
C
O1
O2
O3
500 μM ClW
80 mV
Count/Total
Current (pA)

Figure 3

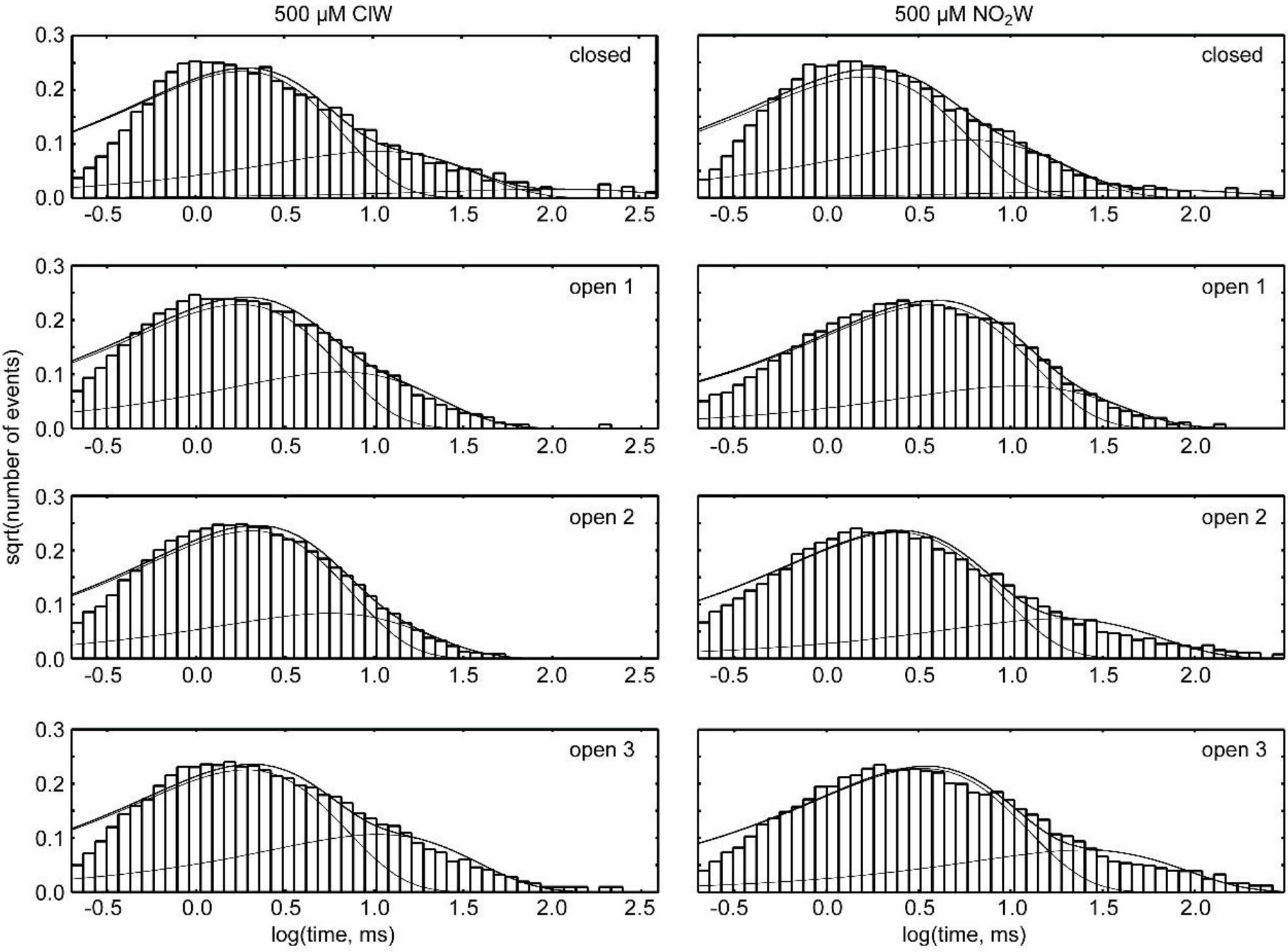
500 µM ClW
500 µM NO2W
closed
open 1
open 2
open 3
sqrt(number of events)
log(time, ms)
0.0
0.1
0.2
0.3
-0.5
0.0
0.5
1.0
1.5
2.0
2.5

Figure 4

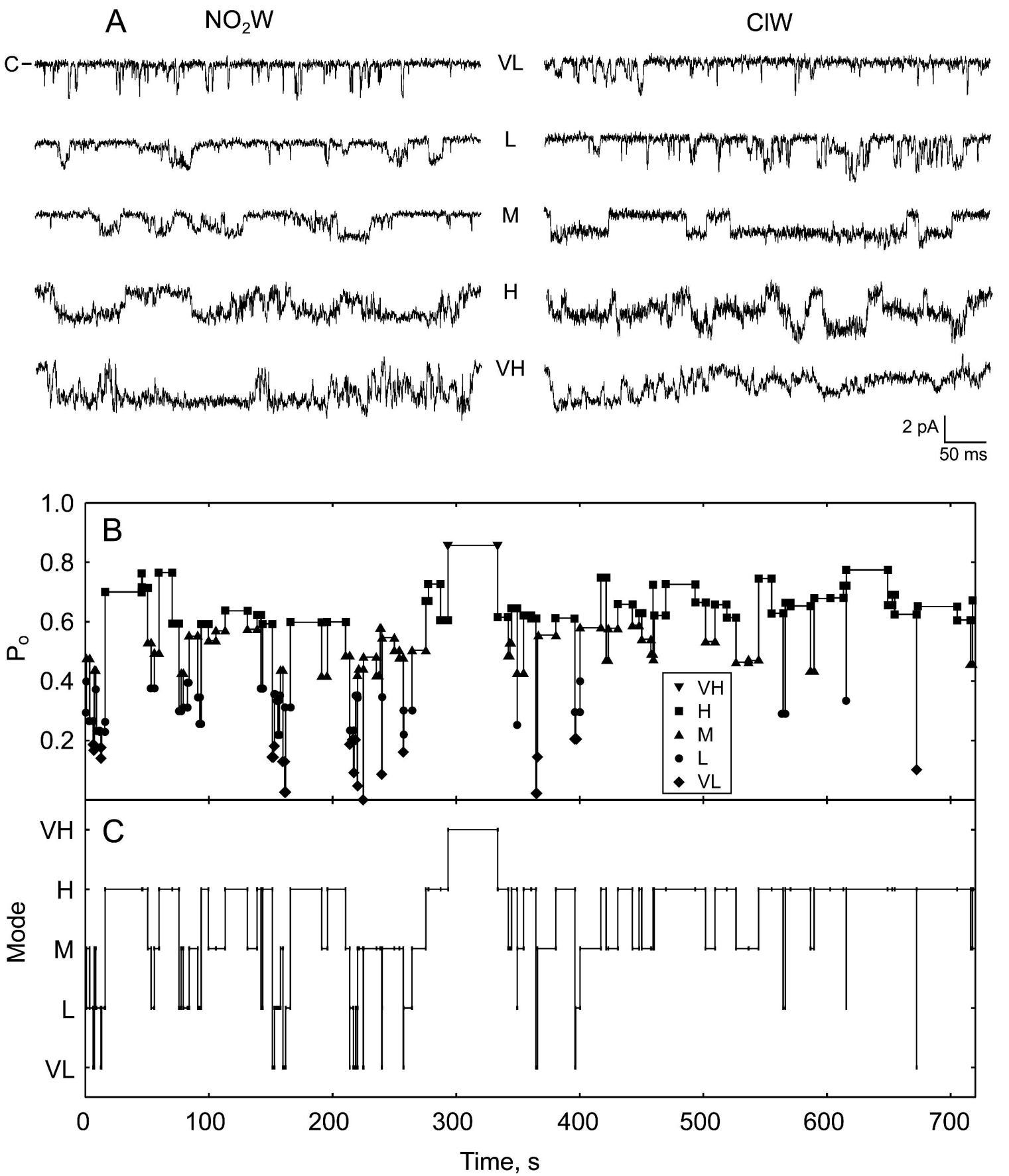
A
NO2W
ClW
C
VL
L
M
H
VH
2 pA
50 ms
B
Po
1.0
0.8
0.6
0.4
0.2
VH
H
M
L
VL
C
Mode
VH
H
M
L
VL
0
100
200
300
400
500
600
700
Time, s

Figure 5

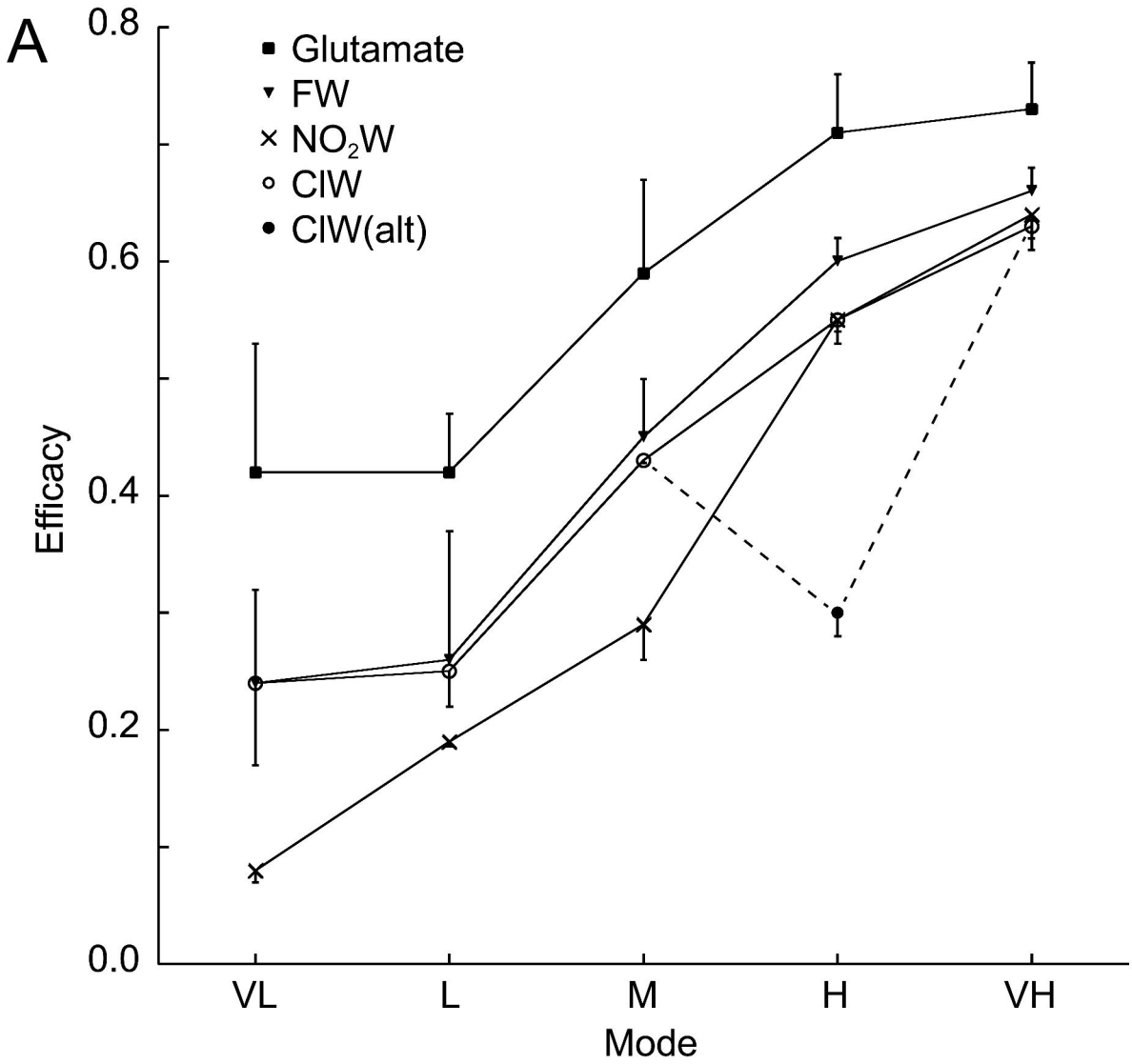

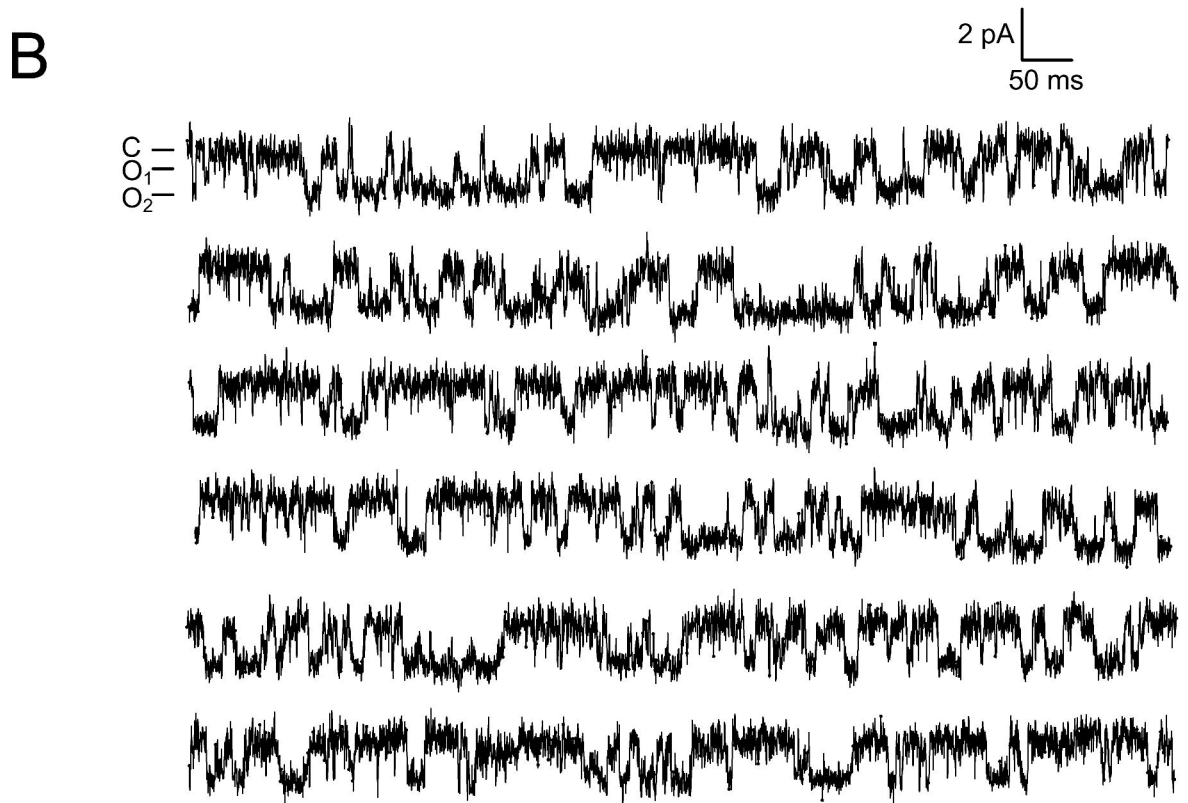

Figure 6

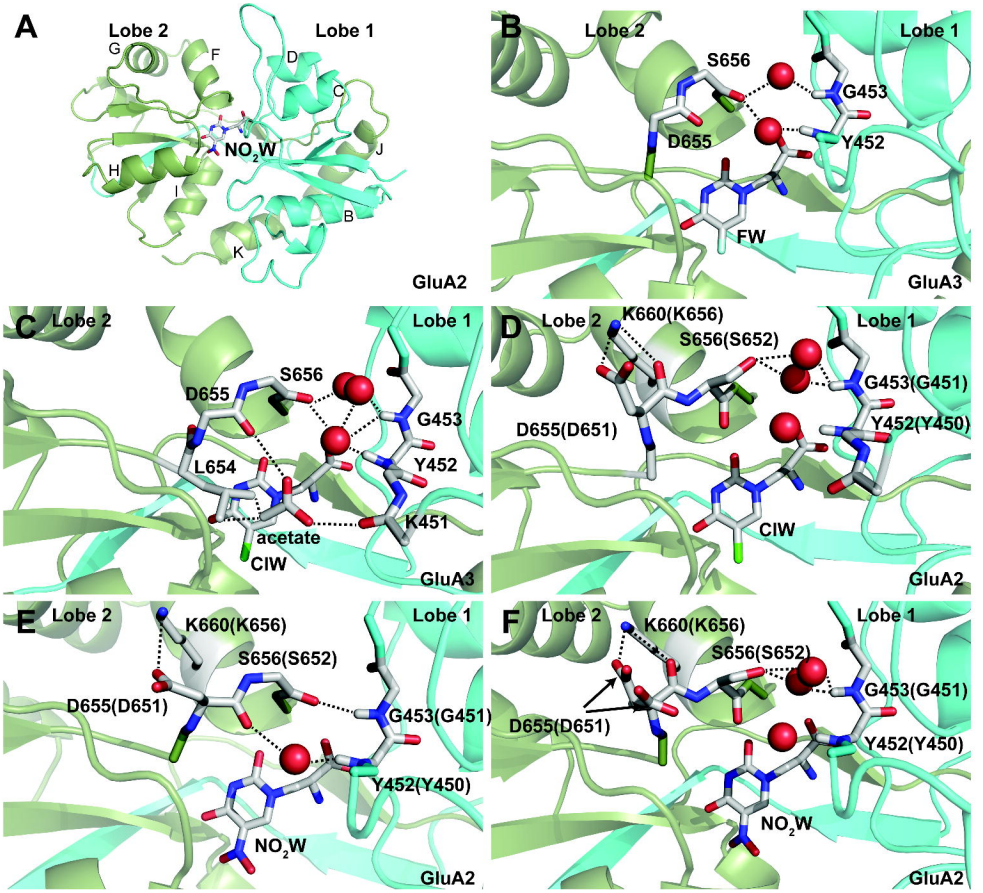
A
Lobe 2
Lobe 1
G
F
D
C
J
H
I
B
K
NO2W
GluA2
B
Lobe 2
Lobe 1
S656
G453
D655
Y452
FW
GluA3
C
Lobe 2
Lobe 1
S656
D655
G453
L654
Y452
K451
acetate
ClW
GluA3
D
Lobe 2
K660(K656)
Lobe 1
S656(S652)
G453(G451)
D655(D651)
Y452(Y450)
ClW
GluA2
E
Lobe 2
K660(K656)
Lobe 1
S656(S652)
D655(D651)
G453(G451)
Y452(Y450)
NO2W
GluA2
F
Lobe 2
K660(K656)
Lobe 1
S656(S652)
G453(G451)
D655(D651)
Y452(Y450)
NO2W
GluA2

Figure 7

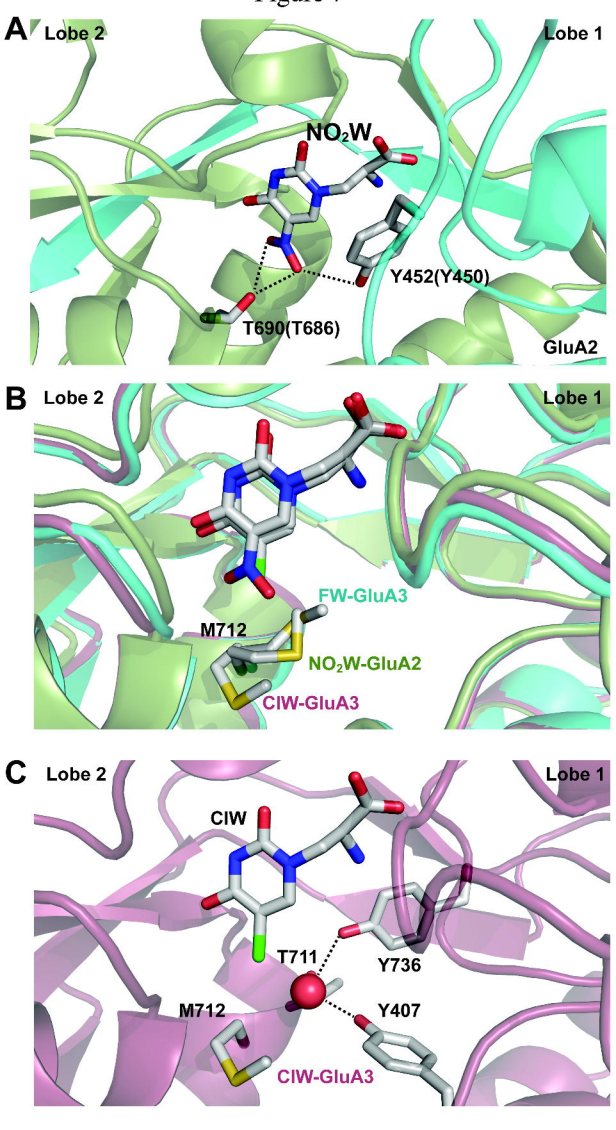
A
Lobe 2
Lobe 1
NO2W
Y452(Y450)
T690(T686)
GluA2
B
Lobe 2
Lobe 1
FW-GluA3
M712
NO2W-GluA2
ClW-GluA3
C
Lobe 2
Lobe 1
ClW
T711
Y736
M712
Y407
ClW-GluA3